Quadrant Analysis of Coherent Structures in Open Channel Flows Over Mobile and Immobile Hydraulically Rough Beds

M.J. Franca[1], B.O. Santos[2], F. Antico[3] and R.M.L. Ferreira[4]

[1] *Laboratoire de Constructions Hydrauliques, École Polytechnique Fédérale de Lausanne, Lausanne, Switzerland, email: mario.franca@epfl.ch*

[2] *Department of Civil Engineering & MARE - Marine and Environmental Sciences Centre, New University of Lisbon, Portugal, email: oliveirasantos@gmail.com*

[3] *Instituto Superior Técnico & CEHIDRO, University of Lisbon, Portugal, email: federica.antico@tecnico.ulisboa.pt*

[4] *Instituto Superior Técnico & CEHIDRO, University of Lisbon, Portugal, email: ruif@civil.ist.utl.pt*

Abstract

Sediment overfeeding may induce important changes in the structure of the near-bed region of gravel-bed river flows, mainly in what concerns exchange of momentum and mass between the flow within the riverbed roughness elements and the flow in the upper regions. Although the turbulent structure of flows over gravel- bed rivers is object of several previous studies, it is not well-known how statistics characterizing coherent turbulence events responsible by the generation of turbulent shear stresses are affected by bed load transport in flows over hydraulically rough beds with low relative submergence. This study is aimed at bridging this research gap. It is based on two-dimensional instantaneous velocity data, in the stream-wise and vertical directions, acquired with Particle Image Velocimetry in a laboratory flume. Two tests simulated framework gravel beds with sand matrixes, one of which fed with sand at near capacity conditions. The framework, immobile under the imposed flow conditions, consists of coarse gravel whose diameters range between 0.5 cm and 7 cm. Matrix and imposed sand feature a median diameter of 0.9 mm. For both tests, the quadrant threshold analysis technique was employed and transported momentum were analyzed and discussed in what concerns their intensity distribution for events in the four quadrants, and for several positions within the flow. It is shown that under mobile bed conditions, sweeps are dominant in the turbulence production in the pythmenic region of the flow. In the outer region of the flow, this is independent from the channel bed; in the overlapping intermediate layer, between the inner region and the pythmenic region, the flow characteristics depend on the position in relation to the crests and troughs of the bed.

1 Introduction

Sediment mechanics, in particular the processes involved in erosion, transport and deposition of sediment particles, greatly depend on local flow hydrodynamics. Sediment transport rates determine river morphodynamics at a wide range of scales and, closing the loop, river morphology influences hydrodynamics, also at a wide range of scales. In spite of the existence of a large body of research on this looping chain of phenomena, fundamental questions remain unsolved in what concerns turbulent flow organization under sediment transport conditions. In particular, the effects of sediment transport on the coherent structures of turbulence that develop on boundary layers, frequently designated as the bursting cycle [24], are still poorly known. Initial interest on coherent structures in wall-bounded flows has been sparkled by the desire to understand the structure of near-wall turbulence and how it determines Reynolds shear stresses and turbulence production ([3], [19], [18], [13], [2]). Following [3], [30] and [20], these coherent structures have been frequently interpreted as events organized periodically in the time domain that imprint its signature on the time series of Reynolds shear stresses, hence the designation of bursting cycle. Conditional sampling techniques, namely quadrant threshold analysis [24], allow for detecting the events of the cycle as interactions of two orthogonal components of the instantaneous velocity, (u_1', u_3') for instance, in the four quadrants of a 2D Cartesian referential. Usual terms are: outward interaction (Q1, $u_1' > 0$, $u_3' > 0$), ejection (Q2, $u_1' < 0$, $u_3' > 0$), inward interaction (Q3, $u_1' < 0$, $u_3' < 0$) and sweep (Q4, $u_1' > 0$, $u_3' < 0$). Ejections and sweeps entail quite different flow kinematics but both contribute to the increase of the absolute magnitude of Reynolds shear stresses.

A considerable body of research has been dedicated to understand the formation of coherent structures in wall- bounded flows, mostly from the study of the dynamics of hairpin vortexes (see [31] and reviews in [22]), and to provide comprehensive experimental and theoretically characterizations [26], [14], including new taxonomies [21], [9].

Specific advances have been achieved in the experimental characterization of flows over hydraulically rough beds, employing Acoustic Doppler Velocimetry (ADV, ADVP), Laser Doppler Anemometry (LDA) or Particle Image Velocimetry (PIV). Investigating flow over gravel beds under moderate relative submergence with ADVP, [23] found out that sweeps are produced dominantly within the interfacial region centered on the plane of the crests of roughness elements, in which the velocity profiles are inflectional. They also found that space-averaged value of mean momentum carried by ejections becomes less relevant towards the bed, relatively to that of sweeps. Analyzing ADV measurements of flows over gravel beds with $k_s/h = 18$ (where k_s is the length scale of roughness elements), [4] conformed the result that ejections become less relevant near the

bed, relatively to sweeps; however, contrarily to [23] they found that the momentum transported by ejections decreases fast below the plane of the crests.

Less information is available for hydraulically rough flows with small relative submergence. PIV data of [16] seems to indicate that, in these flows, larger-scale flow structures are formed by superimposition and coalescence of numerous smaller structures, which confirms the generality of the model of [31]. Performing a Galilean decomposition [1], [16] and [17] observe that shear layers from flow separation in individual roughness elements are the forcing responsible for the instabilities that will ultimately generate coherent structures, which is compatible with the findings of [23] for larger relative submergences.

The link between sediment transport and coherent structures associated to a bursting cycle was pointed out early in the study of [13]. Concerning this issue, advances were accomplished by [15], employing LDA to measure flow statistics over a smooth sand bed. They observed that the presence of intense intermittent sediment transport increases the extreme values of shear stress while the flow becomes more organized in the second and fourth quadrants, mainly increasing the importance of sweep events to turbulence production. The period between events of the second and fourth quadrants (shear stress producing events) decreases considerably in the presence of sediment transport, producing more frequent ejection and sweep events.

More recently, [8], explored an LDA database of flows hydraulically over hydraulically rough beds, mobile and immobile, under moderate relative submergences enough to exhibit a logarithmic layer. They found that the momentum transported by very strong sweeps and also by extreme ejections increase in the mobile bed case. However they found no important differences in the duration and frequency of the events. A general trend of increase of relative importance of sweep events towards the bed was registered. Studying flows over hydraulically rough beds at threshold conditions with ADV, [5] confirm that in the near-bed flow region sweeps become the dominant mechanism for sediment entrainment. They also confirm that the duration and frequency of Q2 and Q4 is smaller in mobile beds in is the smooth-bed case of [15].

The purpose of this work is to contribute to the understanding of coherent structures that develop in gravel-bed channels with low relative submergence and to assess the influence of sand transport on the dynamics of these structures. The study is dedicated to all four types of events in the bursting cycle that contribute to the of Reynolds shear stresses. The joint study of flows over framework-supported gravel beds with low relative submergence and sand transport constitutes the key novelty. Under these conditions Townsend's wall similarity [29] is not likely to hold, indicating that shear stress producing mechanisms may differ from those of high relative submergence. This research addresses also the effect of sand transport within the random array of surface roughness elements, namely its potential to disrupt the mechanisms triggering instabilities.

To accomplish the proposed objective, laboratory flume tests were conducted and 2D instantaneous velocity fields (streamwise and vertical directions) were measured with PIV. The flow is studied based on a quadrant threshold analysis described by [24] and modified by [8]. Mean values and histograms of event duration, maximum shear stress, transported momentum and period of occurrence of all the four types of events were quantified. The sensitivity of the transported momentum to the sampling threshold the events is herein presented and discussed, allowing a physical insight on the influence of the occurrence of sediment transport on the turbulence organization of flows over gravel-bed beds. Further and complementary results on the statistical analysis of shear stress events, ensuing from the very same experiments, may be found in [28], and further details on the experimental tests and data analysis can be found in [27].

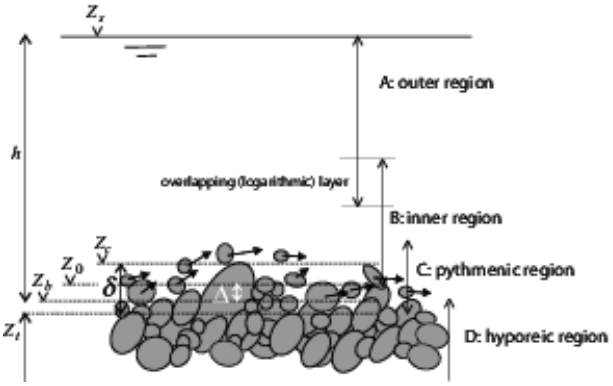

Figure 1: Flow structure proposed for permeable rough porous poorly sorted gravel-sand beds with sediment bed load. h stands for the flow depth, Z_b stands for the boundary zero elevation, Z_c stands for the highest crest elevation, Z_s stands for the elevation of the free-surface and Z_t is the elevation of the deepest through

2 Characterization of the Physical System

The model proposed in [6] for the vertical flow structure of permeable, rough porous poorly sorter, gravel-sand beds with sediment load is herein considered (Figure 1). It features a flow layer, the pythmenic region, where the flow is determined by the particular geometry of bed roughness elements and, possibly, the amount and size of moving particles. Different flow regions overlap as the phenomena that characterizes them does not cease to exist abruptly. The overlapping layer between the pythmenic and inner regions, near the crests of the roughness elements, is assimilable to the "jet layer", as described by [11] or the layer where instabilities leading to coherent structures are generated [16]. Also, interaction of characteristics from both pythmenic and inner regions generates strong momentum fluxes in vertical and spanwise directions [7].

In the inner region, the flow is directly governed by the bed roughness in its lowermost region and indirectly in its uppermost region. It is assumed that the friction velocity is the velocity scale responsible for the momentum transfer from the outer to the inner layer, thus valid for both flow regions [25], [8].

3 Experimental Setup and Methods

3.1 Laboratory Facilities

Experimental tests were performed recurring to the Recirculating Tilting Flume (CRIV), at the Laboratory of Hydraulics and Environment of Instituto Superior Técnico, Universidade de Lisboa. The flume has a rectangular cross section 408 mm wide, 500 mm height, and effective length of 12.5 m. It is composed of ten 0.5 m height glass panels, in each sidewall, that allow acquiring experimental data recurring to flow visualization. The flume slope is adjustable between $-1/200$ and $+1/40$, by means of a motorized system.

The recirculation is made through a pressure circuit, incorporating a centrifugal pump with a maximum discharge of 220 m^3/h. Free surface oscillations are eliminated at the inlet by means of a wooden board. The water level and uniform flow conditions in the subcritical regime were set and controlled by a venetian blind gate at the outlet which is tuned using a screw pole.

At a distance of 2.5 m downstream from the inlet, a conveyor belt imposed a constant sediment feed. The belt was equipped with a structure that allowed controlling the sediment discharge by regulating its velocity and the thickness and width of the sediment streak. A polystyrene board was used to eliminate any free surface disturbance resulting from the introduction of sediments in the stream.

3.2 Measuring Instrumentation

The experimental tests required measurements of free surface elevation, bed topography and instantaneous flow velocity maps in both longitudinal and vertical directions. The free surface elevation and bed topography profiles were obtained with a point gauge with 0.1 mm of precision. Flow discharge in the system was measured by an electromagnetic flow-meter inserted in the recirculating circuit. Instantaneous flow velocity maps were acquired non-intrusively by means of a PIV system. The PIV encompasses a 30 mJ Nd:YAG 532 mm double-cavity (pulsed) laser, a CCD camera with a resolution of 1600×1200 pixel and an acquisition system. The laser is shaped through cylindrical lenses providing a 2 mm thick light sheet. The system operation is performed with time between pulses and sampling frequency controlled by the user. Spurious velocity data were despiked using the phase-space thresholding method [12], adapted for PIV data.

3.3 Characterization of the Tests

Two tests were performed, for which instantaneous flow velocity maps were collected under uniform subcritical flow conditions. The tests were named S3 and S4, respectively in mobile bed and immobile bed conditions, and their main defining parameters are shown in Table 1.

In Table 1, Q stands for flow discharge, i is the bed slope and q_b is the volumetric sediment discharge. The bed is composed of gravel and sand with mean diameter and the geometric standard deviation respectively, $d_{50}^g = 28$ mm, $\sigma_D^g = 1.4$ for gravel (^{g}) and $d_{50}^s = 0.9$ mm, $\sigma_D^s = 1.6$ for sand (^{s}). In both tests the coarse-gravel elements forming a stable framework whose interstices were filled with a sand matrix. This was achieved by water-working the bed for 30 hours to completely assure armoring conditions. By filling the interstices, the thickness of the pythmenic layer is reduced and consequently the porosity in the substratum is reduced too. In test S4 the filling sand is well stored below crests ensuring that sediment transport is completely inexistent under the imposed flow conditions, while in test S3 the sand presence in the bed was slightly increased, until the sand discharge achieves transport capacity.

Table 1: Main characteristics of the experimental tests

Test	Q(l/s)	i(-)	q_b(l/s)	h(m)
S3	23.3	0.0044	4.77×10^{-3}	0.127
S4	16.7	0.0044	2.08×10^{-3}	0.156

Table 2: Main characteristics of the experimental tests

Test	Z_t(m)	Z_c(m)	δ(m)	φ_m(-)	λ_b(-)
S3	0.107	0.146	0.039	0.7197	0.22
S4	0.090	0.144	0.053	0.6570	0.34

The channel bed is characterized by the parameters shown in Table 2, namely the elevations of the planes of the lowest troughs, Z_t, and highest crests, Z_c, the thickness of the pythmenic layer, $\delta = z_c - z_t$, the bed porosity, λ_b and the depth-averaged value of the void function (between Z_t, and Z_c), φ_m, which characterizes the fraction of space that is occupied by the fluid between Z_t, and Z_c.

Variables in Table 3 are Z_s the free surface elevation, while $h*$ is a reference flow depth for shear stress calculation purposes and is calculated as $h* = h - \delta(1 - \varphi_m)$ (details in [7]), U is the depth averaged mean flow velocity in the stream direction, calculated by $U = \frac{Q}{B(Z_s - Z_c)}$, where B is the flume width. The value of τ_0 stands for total shear stress and it is estimated from total shear stress profile. This profile is subjected to a liner regression in the linear segment and then extrapolated to the level of the mean void function, estimating total shear stress of the flow, τ_0, while $u* = \sqrt{\frac{\tau_0}{\rho^w}}$, where ρ^w is the water density.

Non-dimensional parameters Froude, Reynolds and Shields numbers are presented in Table 4. Froude number is calculated by $Fr = \frac{U}{\sqrt{gh}}$, where g is the acceleration of gravity. The Reynolds number is $Re = \frac{Uh}{\nu}$, where ν is the kinematic viscosity of the water. The Shields parameter is calculated for both gravel and sand sizes by $\theta^i = \frac{{u^*}^2}{(\rho^i/\rho^w - 1) g d_{50}^i}$, where u^* stands for friction velocity, ρ^w is the water density, ρ^i is sand or gravel density, and d_{50}^i is the mean diameter of sand or gravel.

Table 3: Flow characteristics

Test	Z_s(m)	h^*(m)	U(m/s)	τ_0(Pa)	u^*(m/s)
S3	0.234	0.116	0.648	3.060	0.057
S4	0.246	0.137	0.557	3.924	0.062

Table 4: Non-dimensional parameters

Test	Fr	Re	θ^g	θ^s
S3	0.61	76606	0.008	0.223
S4	0.45	86843	0.009	0.269

Table 5: Criteria for the detection of shear events

Outward interactions:
$Q_{out} = \{u', w' \in \mathbb{R} : u' > 0 \wedge w' > \frac{\sigma_h}{u'} \wedge u' < \sigma^+\}$

Ejections:
$Q_{ej} = \{u', w' \in \mathbb{R} : u' < 0 \wedge \{w' > \frac{\sigma_h}{|u'|} \vee u' < \sigma^-\}\}$

Inward interactions:
$$Q_{in} = \begin{cases} u', w' \in \mathbb{R} : \\ \{u' < 0 \wedge w' < 0 \wedge |w'| > \frac{\sigma_h}{|u'|} \wedge u' > \sigma^-\} \end{cases}$$

Sweeps:
$$Q_{sw} = \begin{cases} u', w' \in \mathbb{R} : \\ \{u' > 0 \wedge \{\{w' < 0 \wedge |w'| > \frac{\sigma_h}{u'}\} \vee u' > \sigma^+\}\} \end{cases}$$

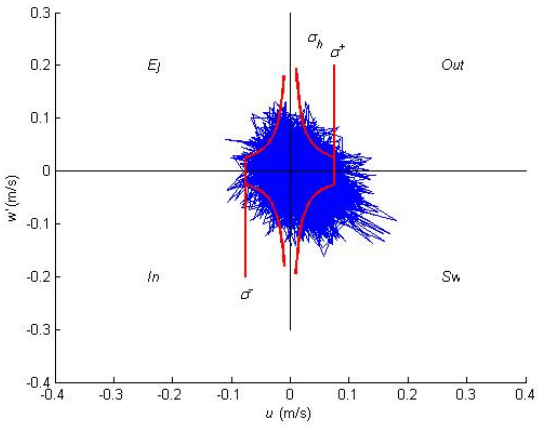

Figure 2: Location of the reference points considered in test S3, in mobile bed conditions

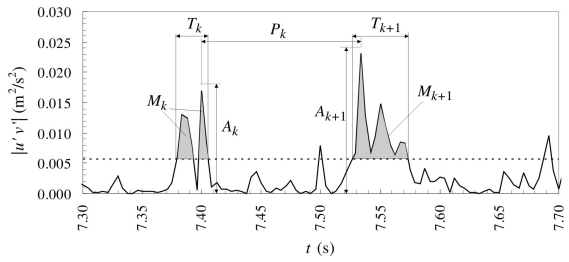

Figure 3: Detailed shear stress time series with parameters that characterize events

4 Data Analysis

4.1 Event Detection

Conditional sampling organizes the shear stresses and helps in the identification of events occurring in the bursting cycle. The quadrant threshold method [24] was chosen as the detection criteria in the modified version proposed by [8]. It involves thresholding $u'w'(t)$ data accordingly to each quadrant, where $u' = u'_1$ and $w' = u'_3$ are the longitudinal and vertical velocity fluctuations, respectively. The thresholds are controlled by the constants

$$\sigma_h = H \times u_{rms} \times w_{rms} \quad (1)$$

$$\sigma^{\pm} = \pm 2.5 \times u_{rms} \quad (2)$$

where H represents the hole size and, u_{rms} and w_{rms} are the root mean square of the instantaneous flow velocity, respectively in longitudinal and vertical directions. The thresholds σ^+ and σ^- depend on the values of the fluctuation of the instantaneous flow velocities and are kept constant for each of the experiments. Outward interactions, ejections, inward interactions and sweeps are identified based on the domains of occurrence described in Table 5.

An example of the distribution of instantaneous velocity fluctuations over the four quadrants with the threshold criteria superimposed is shown in Figure 2. Treating consecutive events of smaller scale as independent events may result in an incorrect approach. To avoid that in the boundary regions, a consecutive set of smaller scale events is eligible as a single major event if the persistence of u' is well correlated with the persistence of the event, as proposed in [8]. This is the justification for the introduction of the additional criterion employing constants $\sigma^+ +$ and σ^-.

4.2 Event statistics

After performing the event detection, the following statistical parameters can be calculated as presented in Figure 3: maximum shear stress (A), transported momentum (M), duration (T) and period (Pc), the time between consecutive events, measured between centroids of the regions representing transported momentum.

Hereinafter, the ensemble-average, over the detected events, of the transported momentum (M) relative to the four types of events will be analysed as a function of the threshold hole for the event detection. A discussion of the remainder statistical parameters is made in [28].

Event detection and calculation of M_k of each event are made inside a loop that goes through a continuous increase of the hole size value, H, starting in zero and ending in 3 with a step of 0.1

4.3 Analyzed positions

The cumulative values of the transported momentum are normalised by the total transported momentum of the correspondent spatial position (m;n) which was produced during the entire experiment. This approach compares the persistence of each kind of event in the experiment sample. The analysis was made at several positions of the flow velocity longitudinal maps as represented in Figure 4. The points considered were chosen accordingly to the physical system proposed by [6], presented earlier in Section 2. Five positions are herein presented in detail: (1,4), (3,2), (3,3), (5,3) and (5,4). These five points stand in different regions of the flow and are representative of these.

The point marked as (1,4) was adopted because it is far enough from the bed. Point (3,2) and (3,3) are standing at the crest level at the interface between inner and pythmenic layers, over the crest level in the overlapping

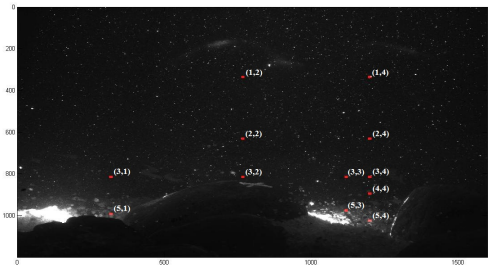

Figure 4: Location of the reference points considered in test S3, in mobile bed conditionss

between inner and pythmenic regions the former, and over the trough position the latter. They allow for evaluating the influence over the flow, caused by the crest itself and by the mobile bed effects. The behaviour in the lower pythmenic region is assessed by investigating points (5,3) and (5,4).

5 Presentation and Discussion of Results

5.1 In the Outer Region, Position (1,4)

In the outer region, the evaluation of the hole size shows that the flow is mainly governed by ejection events. The sweep events also stand out but those are not as important as ejection events in the turbulence production processes. Comparing Figure 5(a), without bed load, to Figure 5(b), where bed load is present, one finds that there is no effect sediment movement at this upper flow region. Although wall similarity is not expected with this low relative submergence, one must assume that the mechanisms that govern coalescence of smaller vortices should be the same at these flow elevations.

5.2 Over the crest, in the overlapping between inner and pythmenic regions, position (3,2)

Figure 6(a) and Figure 6(b) show the shear stress over the crest in the nearest measured point, respectively, for immobile and mobile bed conditions. According to [23] or [16], it is in this layer that instabilities leading to coherent structures are formed. Figure 6(a) and Figure 6(b) show that the importance in the shear stress production processes is transferred from ejection and sweep events to outward and inward events, which expresses a tendency to turbulence isotropy. This is the situation for both cases of immobile and mobile bed conditions.

5.3 At the crest level but over the trough, position (3,3)

This reference point stands in the overlapping between inner and pythmenic regions but over a trough where a shear layer is seen to develop [7]. The quadrant threshold analysis at this point highlights a clear reorganization of the flow, with ejection and sweep events equally responsible for the production of Reynolds shear stresses. The mobile bed does not seem to affect the flow organization at this level, over the trough as it is presented in Figure 7(a) and Figure 7(b), respectively for immobile bed and mobile bed conditions.

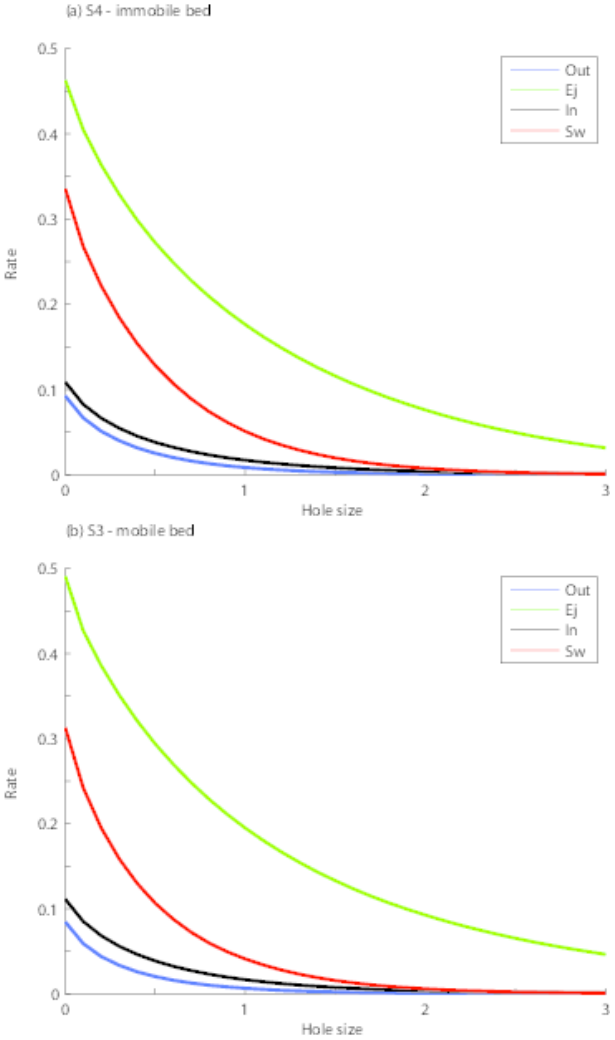

Figure 5: Distribution of transported momentum through the hole size in position (1,4)

5.4 In the pythmenic region, position (5,3)

At this point, standing in the pythmenic region, considering immobile bed conditions, the ejection and sweep events share importance in shear stress production processes. However, when in mobile bed conditions, the ejection events decrease its contribution to the shear stress production processes while sweep events stand out and assume a main role in the same processes as shown in Figure 8(a) and Figure 8(b), respectively for immobile bed and mobile bed. For the immobile bed test (S4) there is relative tendency to isotropy when compared to the mobile bed situation (S3).

5.5 In the lower pythmenic region, position (5,4)

Figure 9(a) and Figure 9(b), respectively standing for immobile and mobile bed conditions, show the sensitivity analysis of the transported momentum to the hole size in the deepest trough. At this (relatively deep) level, the flow exhibits characteristics of both the hyporheic and pythmenic regions. Figure 9(a) shows that in immobile bed conditions, the sweep events assume the major contributions to the shear stress production processes, and they even increase their contribution in the mobile bed case, as shown in Figure 9(b). However, in immobile

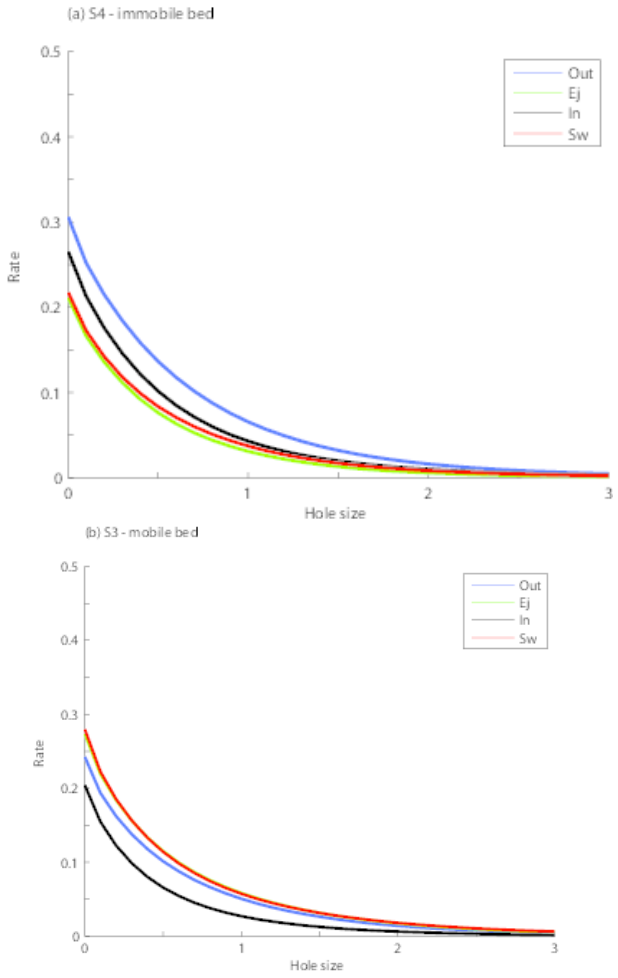

Figure 6: Distribution of transported momentum through the hole size in position (3,2)

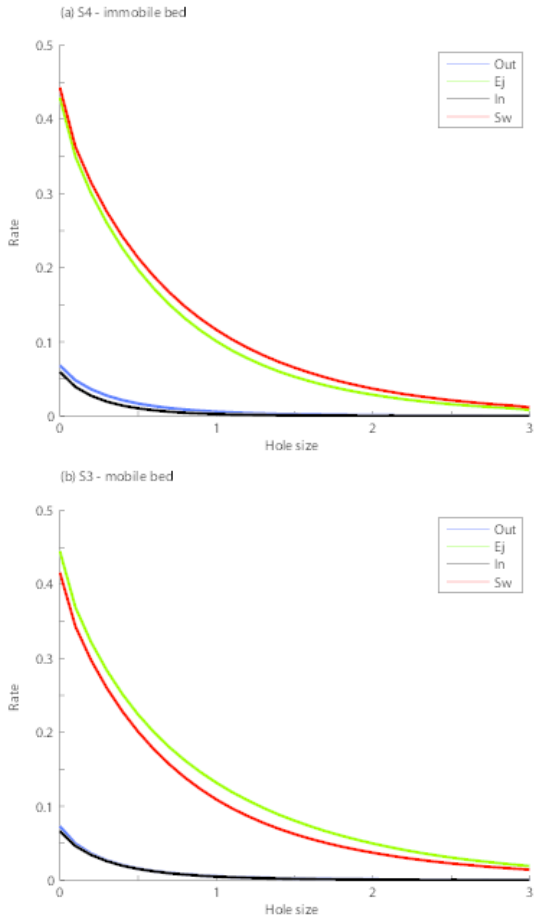

Figure 7: Distribution of transported momentum through the hole size in position (3,3)

bed conditions, contributions from ejection and inward events cannot be neglected at all as they stand out from the outward events. Despite that this reference point is placed in front of a pebble, the flow presents characteristics similar to those found at other reference points placed in the trough, however it is clearer at this reference point, if it is compared for instance with the reference point shown previously in Figure 8(b), where sweep events assume clearly the main contribution to the shear stress production, when in mobile bed conditions.

6 Conclusions

The analysis of laboratorial data, based on instantaneous flow velocity fields, permitted the evaluation of the effect of sediment transport in the near-bed region on the bursting cycle. The two tests were performed in conditions of open-channel flow with porous rough bed and poorly sorted gravel-sand mixture. After the application of a modified quadrant analysis method to sample shear events, statistics of these latter were computed. An analysis of the sensitivity of the transported momentum to the hole size defined to sample the events allowed an inner insight to the shear activity within the flow column.

In the outer layer of the flow, as expected (cf. [5]), the flow is controlled by near-surface conditions and is independent of the channel bed. In the overlapping layer, between inner and pythmenic regions, standing over a crest, the turbulent flow tends to isotropy. The events are equally distributed between the four quadrants and exhibit an equal share in the processes of shear stress production. In the pythmenic region, standing over a trough, mobile bed conditions lead to a situation where ejection and sweep events are responsible for the shear stress production processes with sweep events assuming the main role (cf. [23]), in opposition to the situation in the upper regions of the flow. The mobile bed does not seem to affect the flow organization at this level, for both situations, standing over a crest or over a trough. Ejection events suffer the most important decrease due to sediment transport in the near bed region, more specifically in the pythmenic region. Here, the immobile bed showed a relative tendency to isotropy when compared to the mobile bed situation. In the overlap between hyporheic and pythmenic regions, in mobile bed conditions the sweep events assume the major production of shear stress as pointed out by [5]. In immobile bed conditions, contributions from ejection and inward events cannot be neglected at all as they stand out from the outward events. Although the results here are not conclusive for all positions in the lowest layer, sweeps tend to be here the dominant shear event confirming the observations by [11].

Complementary results, obtained for the same experiments, are shown in [28]. Here it is shown that, generally, the sediment transport of sand decreases the transported momentum and maximum shear stress values (as observed by [5]) but increases their frequency of occurrence in time. The analysis of the probability distri-

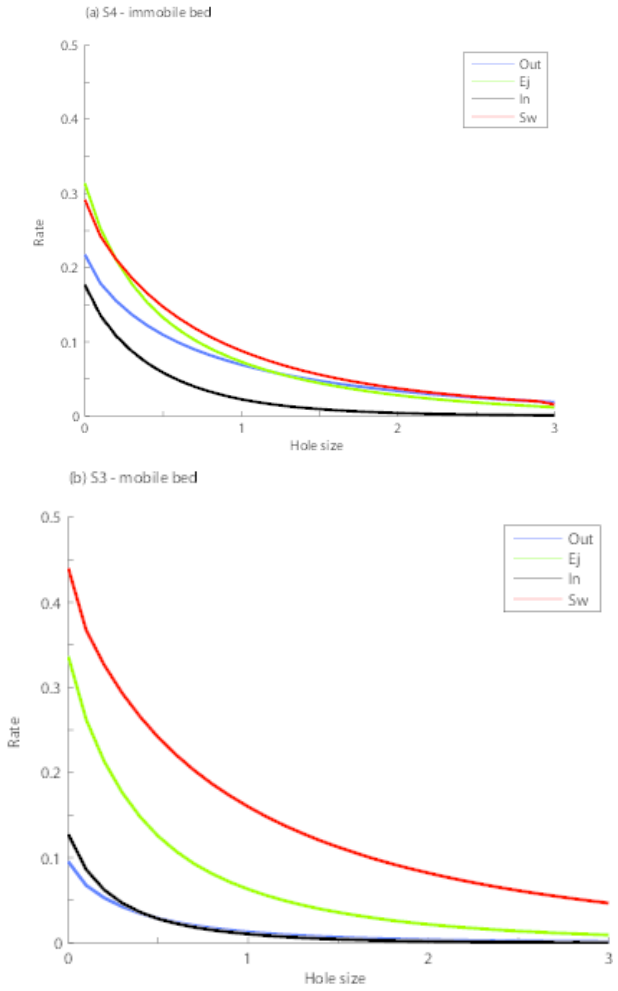

Figure 8: Distribution of transported momentum through the hole size in position (5,3)

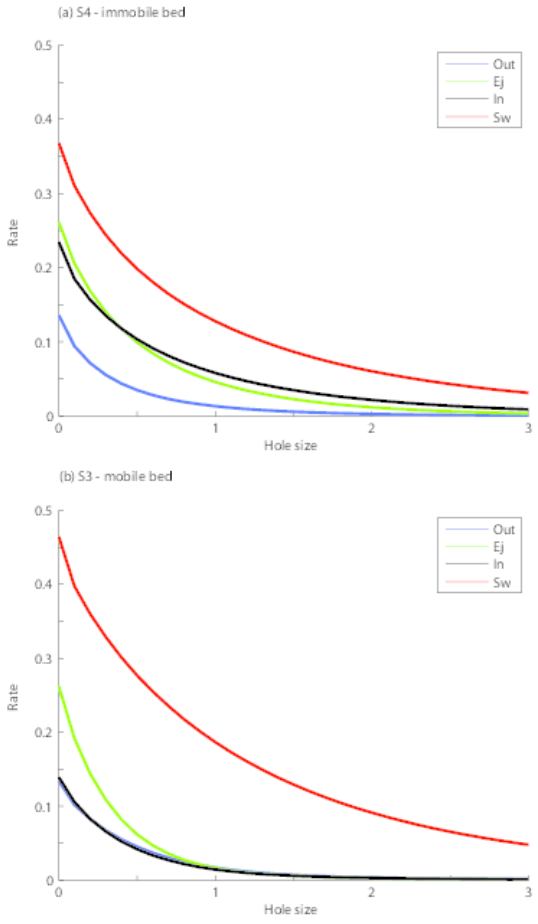

Figure 9: Distribution of transported momentum through the hole size in position (5,4)

bution function of both ejections and sweeps, shows an effect of sediment transport in the reduction of the frequency of large events and in the increase of the frequency of small events. This may be due to breaking of eddy coherence by sediment motion and is especially observed in the pythmenic region.

Acknowledgements

This work was funded by FEDER, program COMPETE, and by national funds through Portuguese Foundation for Science and Technology (FCT) project RECI/ECM-HID/0371/2012 and by the People Programme (Marie Curie Actions) of the European Union's Seventh Framework Programme FP7/2007-2013/ under REA grant agreement n° 607394-SEDITRANS.

References

[1] Adrian, R.J., Christensen, K.T. and Liu, Z.C. 2000. Analysis and interpretation of instantaneous turbulent velocity fields. Exp. Fluids 29: 275-290.

[2] Antonia, R.A. & Atkinson, J.D. (1973). High-order moments of Reynolds shear stress fluctuations in a turbulent boundary layer. J. Fluid Mech. 58(3): 581-593.

[3] Corino, E. R. and R. S. Brodkey (1969). A visual investigation of the wall region in turbulent flow. Journal of Fluid Mechanics, 37(01), 1-30.

[4] Dey, S. and Das, R. (2012) Gravel-Bed Hydrodynamics: Double-Averaging Approach. J. Hydraul. Eng, 138(8): 707-725.

[5] Dey, S., Sarkar, S., Solari, L. (2011). Near-Bed Turbulence Characteristics at the Entrainment Threshold of Sediment Beds. J. Hydr. Engng. 137(9): 945-958.

[6] Ferreira, R. M. L., M. J. Franca, J. G. A. B. Leal, & A. H. Cardoso (2012). Flow over rough mobile beds: Friction factor and vertical distribution of the longitudinal mean velocity. Water Resources Research 48(5):W011126.

[7] Ferreira, R.M.L., Ferreira, L.M.; Ricardo, A.M.; and Franca, M.J. (2010) Impacts of sand transport on flow variables and dissolved oxygen in gravel- bed streams suitable for Salmonid spawning. River Research and Applications 26(4): 414-438.

[8] Ferreira, R.M.L., Franca, M.J.; Leal, J.G.B. and Cardoso, A.H. (2009). Organized turbulence over mobile and immobile hydraulically rough boundaries. In proc. 35 rd IAHR Congress, Vancouver, British Columbia, Canada, pp. 36-43.

[9] Franca, M. J. & Lemmin, U. (2014). Detection and reconstruction of large - scale coherent flow structures in gravel - bed rivers. Earth Surface Processes and Landforms, DOI: 10.1002/esp.3626.

[10] Franca, M. J., Ferreira, R. M., & Lemmin, U. (2008). Parameterization of the logarithmic layer of

double-averaged streamwise velocity profiles in gravel-bed river flows. Advances in Water Resources, 31(6): 915-925.

[11] Gimenez-Curto and Corniero Lera (1996) Oscillating turbulent flow over rough surfaces. J. Geoph. Res. 101(C9): 20745-20758.

[12] Goring, D. G. and Nikora, V.I. (2002). Despiking acoustic doppler velocimeter data. Journal of Hydraulic Engineering 28(1): 117-126.

[13] Grass, A. J. (1971). Structural features of turbulent flow over smooth and rough boundaries. Journal of Fluid Mechanics 50(02): 233-255.

[14] Green, M.A.; Rowley, C.W. Haller, G. (2007) Detection of Lagrangian coherent structures in three-dimensional turbulence. J. Fluid. Mech., 572:111- 120.

[15] Gyr, A. and Schmid, A. (1997). Turbulent flows over smooth erodible sand beds in flumes. Journal of Hydraulic Research 35(4), 525-544.

[16] Hardy, R.J. Best, J.L.; Lane, S.N. and Carbonneau, P.E. (2010) Coherent flow structures in a depth- limited flow over a gravel surface: The influence of surface roughness J. Geophysical Research: Earth Surface, 115(F3006)

[17] Hardy, R.J.; Best, J.L.; Marjoribanks, T.I.; Parsons, D.R.; Rosser, N.J. (2013) Detection and analysis of coherent flow structures in a depth-limited flow over a gravel surface. In "Coherent Flow Structures at Earth's Surface" Ed. by Jeremy G. Venditti, James L. Best, Michael Church and Richard J. Hardy. Wiley-Blackwell. ISBN-13:978-1119962779.

[18] Kim, H. T., Kline, S.T., and Reynolds W.C. (1971). The production of turbulence near a smooth wall in a turbulent boundary layer. Journal of Fluid Mechanics 50(01): 133-160.

[19] Kline, S. J.; Reynolds, W.C.; Schraub, F.A. and Runstadler, P.W. (1967) The structure of turbulent boundary layers. Journal of Fluid Mechanics 30(04): 741-773.

[20] Lu, S.S. and Willmarth W.W. (1973). Measurements of the structure of the reynolds stress in a turbulent boundary layer. Journal of Fluid Mechanics 60(03): 481-511.

[21] Marquis, G.A. and Roy, A.G. (2011) Bridging the gap between turbulence and larger scales of flow motions in rivers. Earth Surface Processes and Landforms 36(4), 563-568.

[22] Marusic, I.; McKeon, B.J.; Monkewitz, P.A.; Nagib, H.M.; Smits, A.J. and Sreenivasan, K.R. (2010) Wall-bounded turbulent flows at high Reynolds numbers: Recent advances and key issues. Phys. Fluids 22, 065103.

[23] Mignot, E.; Hurther, D.; and Barthelemy, E. (2009) On the structure of shear stress and turbulent kinetic energy flux across the roughness layer of a gravel- bed channel flow. J. Fluid Mech., 638(11), 423- 452.

[24] Nakagawa, H. and Nezu, I. (1977). Prediction of the contributions to the Reynolds stress from bursting events in open-channel flows. Journal of Fluid Mechanics 80(01): 99-128.

[25] Pokrajac D.; Finnigan J.J.; Manes, C., McEwan I., Nikora V.I. (2006) On the definition of the shear velocity in rough bed open channel flows. River Flow, vol. 1. Eds R.M.L. Ferreira, E. Alves, J.G.A.B. Leal and A.H. Cardoso. London: Taylor & Francis, p. 89-98.

[26] Porporato, A. and Ridolfi, L. (2002) Some dynamical properties of a differential model for the bursting cycle in the near-wall turbulence. Phys. Fluids 14, 4278.

[27] Santos, B.O. (2013). Coherent structures in open channel flows with bed load transport over an hydraulically rough bed. MSc. Thesis. Faculdade de Ciéncias e Tecnologia, Universidade Nova de Lisboa: http://hdl.handle.net/10362/11204

[28] Santos, B.O., Franca M.J., and Ferreira R.M.L. (2014). Coherent structures in open channel flows with bed load transport over an hydraulically rough bed. In River Flow 2014. Eds. A.J. Schleiss, G. de Cesare, M.J. Franca, M. Pfister.

[29] Townsend A. A. (1976) The structure of Turbulent Shear Flows, 2nd edition. Cambridge University Press, Cambridge, UK.

[30] Willmarth, W.W. and Lu, S.S. (1972). Structure of the reynolds stress near the wall. Journal of Fluid Mechanics 55(01): 65-92.

[31] Zhou, J.; Adrian, R.J.; Balachandar, S. and Kendall, T.M. (1999) Mechanisms for generating coherent packets of hairpin vortices in channel flow. J. Fluid Mech., vol. 387: 353-396.